Nonlinear Dyn (2024) 112:7185–7198
https://doi.org/10.1007/s11071-024-09281-9

ORIGINAL PAPER

Reduction of settling time by multi-frequency pulsed parametric excitation

Miguel Ramírez-Barrios · **Fadi Dohnal**

Received: 30 June 2023 / Accepted: 31 December 2023 / Published online: 8 March 2024

Abstract Introducing a time-periodicity into a system parameter leads to parametric excitation, which in general, may cause a parametric resonance with exponentially increased vibration. Applying a parametric excitation but carefully tuning its frequencies to multiple parametric anti-resonance frequencies is investigated here. The parametric excitation here is realized by an open-loop control at the system boundary that allows for an energy flow into or from the system. A parametric anti-resonance successfully triggers an energy transfer between specific vibration modes of the system and occurs in systems with at least two degrees of freedom. Such an energy transfer increases the overall dissipation of kinetic energy of a lightly damped system. This contribution presents an approach to accelerate the mitigation of transient vibrations by applying a multi-frequency parametric excitation with two or more parametric anti-resonance frequencies. The potential application in a MEMS sensor arrangement consisting of two and more coupled flexible beams exemplifies the method. Starting from the minimum system with two degrees of freedom, the averaging method is applied to analyze the transient slow flow, leading to an analytical approximation of the transition time response of a pulsed multi-frequency parametric excitation system. For a specific example, a reduction of 96.7% of the transient vibrations is achievable.

Keywords Parametric resonance · Floquet theory · Anti-resonance · Vibration control · MEMS systems · Quasi-periodic system

M. Ramírez-Barrios (✉)
Instituto Politécnico Nacional, UPIBI, Av. Luis Enrique Erro S/N, 07738 Mexico City, Mexico
e-mail: mlramirezb@ipn.mx

F. Dohnal
Research Center for Microtechnology, Vorarlberg University of Applied Sciences, 6850 Dornbirn, Austria

1 Introduction

Sensors are utilized in all kinds of applications to measure a multi-physical system's transient and steady states. The design and analysis of dynamics are under investigation and utilized in many different areas ranging from classical engineering [19,33,37] over physics [7] up to environmental and biological engineering [41].

For successful measurements, it is crucial for the sensor that its own dynamics do not distort the measurement. This is achieved by designing fast dynamics of the sensor. The quality factor limits the speed of the sensor response dynamics. A high-quality factor Q is needed to allow for a high sensor sensitivity [20,25]. However, high Q leads simultaneously to a low damping and slow sensor transients. The measurement system must wait for these sensor transients' decay to gain a reliable reading of the system dynamics under investigation, not the sensor dynamics. This contribution highlights a methodology for speeding up the tran-

sient time of a sensor while keeping the advantageous high-quality factor [26].

In the scope of this investigation, we focus on time-periodic systems. Time-periodic systems have been investigated for decades. A time-periodicity can be unavoidable and undesired, e.g. the base excitation of a motor in a ship subject to an external excitation by the sea [16]. A time-periodicity can also be implemented in the context of sensors for exploiting a parametric resonance that amplifies the sensor sensitivity, e.g. the [23,32].

Time-periodic systems, even linear ones, cannot be solved analytically in closed form. However, several analytical techniques exist which allow for an approximate solution. The most commonly applied methods are singular perturbation methods like the multiple scales method [24], the method of averaging [40] or complexification [18], and several textbooks exist that apply them interchangeably [5,35,38]. Both methods rely on the assumption of small bookkeeping parameter ε. It can be shown that for an approximation of first order in ε both methods lead to the same result on the time scale of $1/\varepsilon$. The method of averaging [39] is followed here, specifically in the general case. The benefit of this method was outlined in more detail very recently in [40]. Introducing multiple parametric frequencies in the present work results in a quasi-periodic parametric excitation for which the method of averaging in the general case remains applicable, and the findings in [15] can be built upon.

Time-periodic systems exhibit parametric combination resonances for [9] at which the system vibrations increase, depending on the strength, frequency of the parametric excitation and the system damping. The parameter combinations for which an increase of vibrations is observed lie within the famous Arnould tongues [28] or instability tongues that are visualized in the Ince-Strutt stability diagram [8]. For a multiple-degree-of-freedom-system, instability tongues may appear close to the principal parametric resonance frequencies $2\Omega_i/n$ or at parametric combination resonance frequencies $|\Omega_i \mp \Omega_j|/n$ with $n \in \mathbb{N}$ and Ω_i being the natural frequency of the underlying system without parametric excitation [43].

The numerical stability analysis of time-periodic systems needs particular attention, and several methods were developed in the time domain (Monodromy matrix [27]) and the frequency domain (Hill matrix [4]). Recent developments for single as well as coupled Mathieu equations can be found in [8], also utilizing symplectic properties [27,28]. The quasi-periodic Mathieu equation, the simplest time-periodic system with multiple frequency excitation, was investigated in [31,45], showing very rich dynamics. In the present contribution dealing with a set of coupled Mathieu equations, such rich dynamics were not observed, which is why the treatment by singular perturbation leads to still compact expressions. The numerical analysis of more complex systems with quasi-periodic parametric excitation can be analyzed by following [42].

Under certain conditions, parametric combination resonances can show a stabilizing behaviour observed initially in [36] wherein the combination between a destabilizing self-excitation and a parametric combination resonance led to an overall stable system. This phenomenon was then termed parametric anti-resonance to underline the stabilizing behaviour. This observation was investigated in a series of works analytically and numerically [10–12,14]. These studies showed that not the interaction between self-excitation and parametric excitation leads to vibration mitigation but solely a properly tuned parametric combination resonance ([10]). This triggered the possibility that any vibrating system with at least two degrees of freedom and small damping has the potential to exploit the vibration mitigation by a parametric combination resonance. This finding was confirmed experimentally for several discrete and continuous systems in [13].

MEMS (micro electromechanical systems) are utilized in several applications [2,22] and allow for a simple electrical implementation of a parametric excitation [1,21,26]. During operation, MEMS can be driven to linear or non-linear regimes using different actuation mechanisms [44]. MEMS based on resonators can be composed of coupled structures (mechanically or electrically) in which coupling and energy transfer between vibration modes are analyzed for a specific purpose [17]. This coupling involves various vibration modes of a structure and exploits an intermodal coupling or the internal resonance phenomenon. These represent a nonlinear mechanism for transferring energy from one vibration mode to another [3,6]. Furthermore, these structures can be excited in various ways, in their first mode or higher modes of vibration [34]. MEMS resonators possess diverse dynamics and its potential applications lie in energy harvesting, frequency stabilization in oscillators and synchronization [17]. The present work focuses exclusively on the linear dynam-

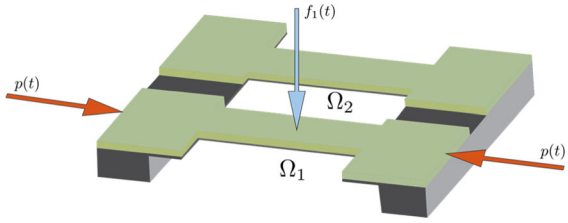

Fig. 1 MEMS schematic diagram base on [26]

ics and achieves modal coupling by a parametric excitation. Introducing a specific parametric excitation leads to a selective modal coupling and consequently to a selective energy transfer between vibration modes as originally shown in [11,14]. Doing so we can trigger a selective modal coupling between the first mode and the remaining modes of the system. The usage of a single frequent parametric excitation for vibration mitigation was investigated theoretically in [29,30] and verified for a MEMS sensor in [25]. Motivated by the results for a MEMS with 2DOF, the configuration is extended here to multiple DOFs, always leading to linearly coupled Mathieu equations. The concept is then generalized to the more complex case of a quasi-periodic parametric excitation at several parametric anti-resonance frequencies. Analytical conditions for a confined pulses of parametric excitations are given for achieving a mitigation of transient vibrations. The first order approximation of the slow flow dynamics is derived by applying the averaging method in the general case [40]. It shown that driving a linear MEMS at different parametric anti-resonance frequencies triggers a continuous energy transfer between selected vibration modes. The benefit for reducing the settling time for MEMS with three, four and more beams is highlighted.

In summary, the averaging technique is applied to a multi-parametric excited NDOF system at the anti-parametric frequency $\Omega_p = |\Omega_i - \Omega_j|$; at this frequency, the averaged system accurately describes the system's dynamics under the influence of anti-parametric excitation. The transfer of energy vibrations between the system modes is achieved when the parametric excitation is tuned at Ω_p. Using these dynamics behaviour, a technique for time-settling reduction is proposed, leading to a 90.39%, 93.13%, 94.44% and 96.79% time-settling reduction for 2DOF, 3DOF, 4DOF and 10DOF, respectively.

2 MEMS

The MEMS considered is sketched in Fig. 1 consisting of two flexible beams that are fixed on both sides to the same frame as presented in [26]. The beam at the bottom is the sensor. The external excitation is indicated by the external forcing $f_1(t)$. The beam on the top is manufactured the same way but is an entirely passive part of the system. The parametric excitation is applied to the sensing beam solely. Due to the physical coupling via the frame, the parametric excitation is also acting on the other beam. Approximating the dynamics of each beam by a single mode and its corresponding natural frequency Ω_i, the equations of motion can be written as

$$\begin{aligned} \ddot{x}_1 + d_1\dot{x}_1 + \Omega_1^2 x_1 + b_{11}p(t)x_1 + b_{12}p(t)x_2 &= f_1(t) \\ \ddot{x}_2 + d_2\dot{x}_2 + \Omega_2^2 x_2 + b_{21}p(t)x_1 + b_{22}p(t)x_2 &= 0 \end{aligned} \quad (1)$$

where the parametric excitation $p(t) = \cos\Omega_p t$ couples the individual systems. Figure 1 depicts the conceptual configuration of the MEMS resonators according to [25,29].

3 Applying averaging method

The coupled Mathieu equations in Eq. (1) without external excitation, i.e. after the measurement time, can be rewritten in a more general form as

$$\ddot{\mathbf{x}}(t) + \mathbf{D}\dot{\mathbf{x}}(t) + \left(\mathbf{\Omega}^2 + \mathbf{B}\cos\left(\Omega_p t\right)\right)\mathbf{x}(t) = 0 \quad (2)$$

where $\mathbf{x}(t)$ is an n vector, $\mathbf{D}$, $\mathbf{B}$ and $\mathbf{Q}$ are $n \times n$ constant matrices. Assuming distinct natural frequencies, we can write the matrix $\Omega^2 = \text{diag}\left\{\Omega_1^2, \Omega_2^2, \ldots, \Omega_n^2\right\}$ being diagonal incorporating the natural frequencies of the undamped system. Adopting the Einstein summation as a notation, where repeated indices are implicitly summed over, Eq. (2) leads to the comprehensive index form

$$\ddot{x}_i(t) + \Omega_i^2 x_i(t) = -\varepsilon\left[\hat{d}_{ij}\dot{x}_i - \hat{b}_{ij}x_i\cos\left(\Omega_p t\right)\right] \quad (3)$$

with $i, j = 1, 2, \ldots$, and where ε is assumed to be a small parameter needed for the singular perturbation that rescales the damping and coupling coefficients in

Eq. (2) according to by $d_{ij} = \varepsilon\hat{d}_{ij}$ and $b_{ij} = \varepsilon\hat{b}_{ij}$. Rescaling the time to normalize the frequency by

$$\tau = \Omega_p t \tag{4}$$

leads to

$$x_i'' + \omega_i^2 x_i = -\frac{\varepsilon}{\Omega_p^2}\left(\Omega_p \hat{d}_{ij} x_i'(\tau) + \hat{b}_{ij} x_i(\tau)\cos\tau\right) \tag{5}$$

where $(\cdot)'$ is the derivative with respect to τ and $\omega_i = \Omega_i/\Omega_p$. Defining the amplitude-phase coordinate transformation

$$\begin{aligned} x_i(\tau) &= u_i(\tau)c_i + v_i(\tau)s_i \\ x_i'(\tau) &= -u_i(\tau)\omega_i s_i + v_i(\tau)\omega_i c_i \end{aligned} \tag{6}$$

using the abbreviations $s_i = \sin(\omega_i\tau)$, $c_i = \cos(\omega_i\tau)$, the equations of motion in Eq. (5) can be rewritten into the so-called quasi-normal form [39]. For the sake of simplicity, the explicit time dependence on τ is not written. Applying this transformation yields

$$-u_i'\omega_i s_i + v_i'\omega_i c_i = \frac{\varepsilon}{\Omega_p^2}\Gamma_i(u_i, v_i, \tau) \tag{7}$$

where the scaled right-hand side reads

$$\begin{aligned} \Gamma_i = &-\Omega_p \sum_j \hat{d}_{ij}\left(-u_j\Omega_j s_j + v_j v_j c_j\right) \\ &- \sum_j \hat{b}_{ij}\left(u_j c_j + v_j s_j\right)\cos\tau \end{aligned}$$

Respecting Eq. (7), Eqs. (5) finally become

$$u_i' = -\frac{\varepsilon}{\Omega_p\Omega_i}\Gamma_i(\mathbf{z},\tau)s_i = \varepsilon M_i^s(\mathbf{z},\tau) \tag{8}$$

$$v_i' = \frac{\varepsilon}{\Omega_p\Omega_i}\Gamma_i(\mathbf{z},\tau)c_i = \varepsilon M_i^c(\mathbf{z},\tau) \tag{9}$$

with vector $\mathbf{z} = \begin{bmatrix} u_1 & v_1 & u_2 & v_2 & \ldots \end{bmatrix}^T$. The functions on the right-hand side $M_i^s(\mathbf{z},\tau)$ and $M_i^c(\mathbf{z},\tau)$ are not quasi-periodic and can be split into a finite sum of periodic terms

$$M_i^s(\mathbf{z},\tau) = \sum_{k=1}^{N} M_{i,k}^s(\mathbf{z},\tau) \tag{10}$$

$$M_i^c(\mathbf{z},\tau) = \sum_{k=1}^{N} M_{i,k}^c(\mathbf{z},\tau) \tag{11}$$

where N is fixed, $M_{i,k}^s(\mathbf{z},\tau)$ and $M_{i,k}^c(\mathbf{z},\tau)$ are T_k periodic functions in τ. For this case, the *averaging in the general case* can be applied Eqs. (8) and (9) resulting in

$$\hat{u}_i' = \varepsilon\sum_{k=1}^{N}\frac{1}{T_k}\int_0^{T_k} M_{i,k}^s(\mathbf{z},\tau)d\tau \tag{12}$$

$$\hat{v}_i' = \varepsilon\sum_{k=1}^{N}\frac{1}{T_k}\int_0^{T_k} M_{i,k}^c(\mathbf{z},\tau)d\tau, \tag{13}$$

where the hat indicates the time-averaged variables and the original $\mathbf{z}(\tau)$ and averaged $\hat{\mathbf{z}}(\tau)$ solutions differ in an order of $O(\varepsilon)$, on the timescale $1/\varepsilon$. Using trigonometric identities, the products of the trigonometric terms can be rewritten as a sum of basic trigonometric terms of which the period T_k can be determined, and the integrals in Eqs. (12) and (13) calculated. Resonant terms occur at this step at frequencies

$$\Omega_p = \frac{2\Omega_i}{n}\ i = 1, 2, \ldots n, \tag{14}$$

and

$$\Omega_p^{ij} = \frac{|\Omega_i \mp \Omega_i|}{n}\ i, j = 1, 2, \ldots n, \text{ for } i \neq j \tag{15}$$

4 Averaging for MEMS with 2-DOFs

Applying the averaging procedure described above to system in Eq. (2) with $n = 2$ at the parametric anti-resonance frequency $\Omega_p^{21} = |\Omega_2 - \Omega_1|$. Namely,

$$\ddot{\mathbf{x}} + \begin{bmatrix} d_{11} & d_{12} \\ d_{21} & d_{22} \end{bmatrix}\dot{\mathbf{x}} + \left(\Omega^2 + \begin{bmatrix} b_{11} & b_{12} \\ b_{21} & b_{22} \end{bmatrix}\cos\left(\Omega_p^{21} t\right)\right)\mathbf{x} = 0 \tag{16}$$

where $\mathbf{x} = \begin{bmatrix} x_1 & x_2 \end{bmatrix}^T$ and $\Omega^2 = \operatorname{diag}\left(\Omega_1^2, \Omega_2^2\right)$, we obtain

$$\hat{\mathbf{z}}_2{}' = \hat{\mathbf{A}}_2\hat{\mathbf{z}}_2 \tag{17}$$

with the coefficient matrix

$$\hat{\mathbf{A}}_{\mathbf{2}} = \frac{1}{\Omega_p^{21}} \begin{bmatrix} -\frac{1}{2}d_{11} & 0 & 0 & \frac{1}{4\Omega_1}b_{12} \\ 0 & -\frac{1}{2}d_{11} & -\frac{1}{4\Omega_1}b_{12} & 0 \\ 0 & \frac{1}{4\Omega_2}b_{21} & -\frac{1}{2}d_{22} & 0 \\ -\frac{1}{4\Omega_2}b_{21} & 0 & 0 & -\frac{1}{2}d_{22} \end{bmatrix} \tag{18}$$

Note that the damping and coupling coefficients are rescaled back according to $d_{ij} = \varepsilon\hat{d}_{ij}$ and $b_{ij} = \varepsilon\hat{b}_{ij}$. The difference between the original solution $\mathbf{z_2} = \begin{bmatrix} u_1 & v_1 & u_2 & v_2 \end{bmatrix}^T$ and the averaged solution $\hat{\mathbf{z}}_{\mathbf{2}} = \begin{bmatrix} \hat{u}_1 & \hat{v}_1 & \hat{u}_2 & \hat{v}_2 \end{bmatrix}^T$ is of order ε, i.e. $\hat{\mathbf{z}}_{\mathbf{2}}(\tau) - \mathbf{z_2}(\tau) = \mathcal{O}(\varepsilon)$ on the time scale $1/\varepsilon$. Tuning the parametric excitation to the parametric anti-resonance frequency $\Omega_p = \Omega_p^{21}$, note that the direct coupling coefficients b_{ii} as well as the off-diagonal damping coefficients d_{ij} do not appear in the first order approximation in Eqs. (18). This fact was already observed in [15]. The slow flow of the system in Eq. (2) at $\Omega_p = \Omega_p^{21}$ is entirely characterized by the coupling terms b_{12} and b_{21}, and the diagonal damping coefficients d_{11} and d_{22}.

The coefficient matrix $\hat{\mathbf{A}}_{\mathbf{2}}$ possesses two repeated eigenvalues $\hat{\lambda}_1^{\hat{\mathbf{A}}_{\mathbf{2}}} = \hat{\lambda}_3^{\hat{\mathbf{A}}_{\mathbf{2}}}$ and $\hat{\lambda}_2^{\hat{\mathbf{A}}_{\mathbf{2}}} = \hat{\lambda}_4^{\hat{\mathbf{A}}_{\mathbf{2}}}$ given by

$$\hat{\lambda}_{1,2}^{\hat{\mathbf{A}}_{\mathbf{2}}} = -\frac{1}{4\Omega_p}\left(d_{11} + d_{22} \pm \sqrt{(d_{11} - d_{22})^2 - \frac{b_{12}b_{21}}{\Omega_1\Omega_2}}\right) \tag{19}$$

They represent the behaviour of the dynamics on the slow time scale which refers to the envelope of the system response in Eq. (18) and is shown in Fig. 2. Therefore, if $\hat{\lambda}_{12}$ are purely real, the response envelope decreases exponentially in time, as shown in Fig. 2a. Alternatively, complex conjugate eigenvalues correspond to a modulated envelope, sometimes called a beating signal as depicted in Fig. 2b. Thus, to determine this nature of the stable response $\hat{\lambda}_{12} \in \mathbb{R}$ or $\hat{\lambda}_{12} \in \mathbb{C}$ it is sufficient to verify the following inequality [10]

$$(d_{11} - d_{22})^2 > \frac{b_{12}b_{21}}{\Omega_1\Omega_2} \geq 0. \tag{20}$$

If this inequality is fulfilled, $\hat{\lambda}_{12}$ are real. Otherwise, $\hat{\lambda}_{12}$ are complex-valued in this case the imaginary part of $\hat{\lambda}_{12}$ can be interpreted as the frequency of the envelope signal

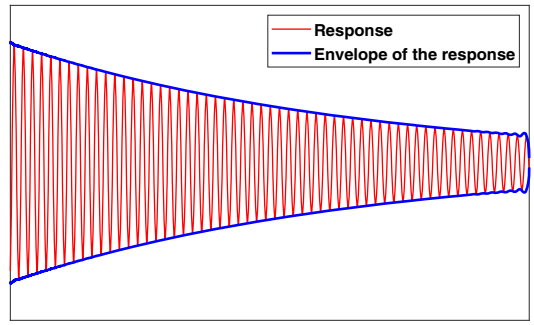

(a) Envelope of the system response for $(d_{11} - d_{22})^2 > \frac{b_{12}b_{21}}{\Omega_1\Omega_2} > 0$.

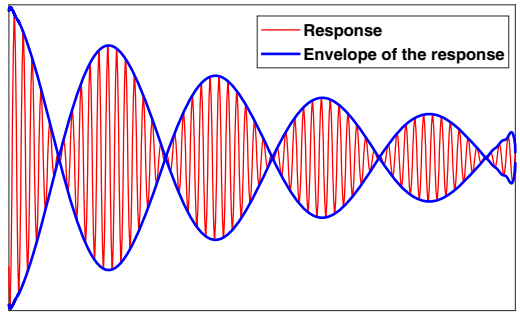

(b) Envelope of the system response for $\frac{b_{12}b_{21}}{\Omega_1\Omega_2} > (d_{11} - d_{22})^2 \geq 0$.

Fig. 2 Characterization of the response envelope of the system in Eq. (16) according to inequality in Eq. (19)

$$\omega_{\hat{\mathbf{A}}_{\mathbf{2}}} = \pm\frac{1}{4\Omega_p^{21}}\sqrt{\frac{b_{12}b_{21}}{\Omega_1\Omega_2} - (d_{11} - d_{22})^2}. \tag{21}$$

Moreover, the two envelope response signals for the system in Eq. (16) are in anti-phase because there are two equal frequencies. Therefore, it is possible to determine the period of the envelope signals in anti-phase. Rescaling the time τ according to Eq. (4) and considering $\omega_{\hat{\mathbf{A}}_{\mathbf{2}}}$ as the frequency, we estimate the period of the slow motion as

$$T_{\hat{\mathbf{A}}_{\mathbf{2}}} = \frac{8\pi}{\sqrt{\frac{b_{12}b_{21}}{\Omega_1\Omega_2} - (d_{11} - d_{22})^2}} \tag{22}$$

Table 1 2DOF system parameters

Ω_i in Mrad/s	$Q\ [\times 10^4]$	b_{ij} in $1/s^2$
$\Omega_1 = 1.8316$	$Q_1 = 4.6964$	$b_{12} = b_{11} = 1.3 \times 10^9$
$\Omega_2 = 1.8390$	$Q_2 = 4.7154$	$b_{21} = b_{22} = 1.2 \times 10^9$

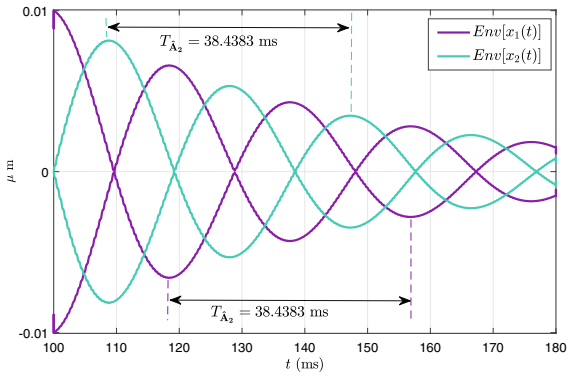

Fig. 3 Envelope of the time responses of the system in Eq. (16) at $\Omega_p^{21} = |\Omega_2 - \Omega_1|$. The analytical prediction in Eq. (22) matches the observed period $T_{\hat{\mathbf{A}}_2}$

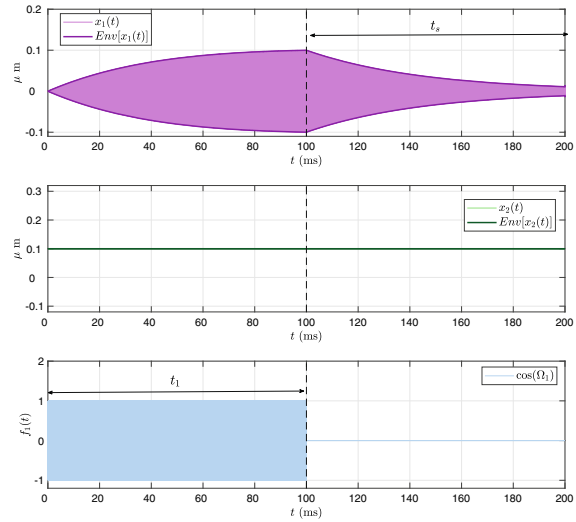

Fig. 4 Time responses of the 2DOF-MEMS in Eq. (1) with a settling time $t_s = 100$ ms

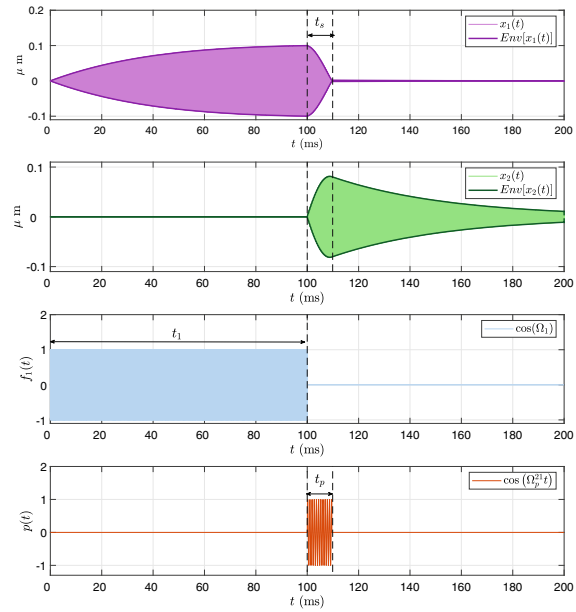

Fig. 5 Time responses of the 2DOF-MEMS in Eq. (1) under the effect of a parametric excitation pulse $t_p = 9.8$ ms. The settling time is reduced to $t_s \approx 9.8$ ms

To highlight the prediction quality of Eq. (22), the simulation of a specific system represented by equations of motion in Eq. (16) is performed. The following system parameter were chosen according to [25,26] and are listed in Table 1 where the quality factors are defined as $Q_1 = \Omega_1/d_{11}$ and $Q_2 = \Omega_2/d_{22}$. The envelopes of the system responses $Env[x_1(t)]$ and $Env[x_2(t)]$ are shown in Fig. 3. The period identified from the numerical simulation $T_{\hat{\mathbf{A}}_2} = 38.4383$ ms coincides with the analytical prediction in Eq. (22). A direct comparison between the solution $\mathbf{x}$ of the original system in Eq. (16) and the solution $\hat{\mathbf{z}}$ resulting from the averaged system is given in the appendix.

5 Pulse of parametric excitation in 2DOF

A continuous parametric excitation at a parametric combination resonance frequency leads to a steady energy transfer between the modes of the system, as discussed in more detail in [14]. Starting with vibration in beam 1, such a continuous excitation results in an energy transfer into beam to within the period estimated in Eq. (22). After this time however, the energy is transferred back, at least what is left after dissipation

within the next period. This back and forth transfer happens continuously until all kinetic energy is eventually dissipated by the damping coefficients of both beams. In order to avoid this back-channeling of kinetic energy from beam 2 to beam 1, we apply the parametric excitation only within a short pulse with time of a single period. The time response of the 2DOF-system subject to an external excitation $f_1(t)$ is shown in Fig. 4. The steady-state of beam 1 is reached after 100 ms. After this measurement, the excitation is switched of and the vibration level of beam 1 decays exponentially due to its damping. Beam 2 is not affected during this operation.

In contrast to this, we apply a parametric excitation right after the measurement time during the short pulse time $t_{p_2} = T_{\hat{\mathbf{A}}_2}/4$ given in Eq. (22). This operation is highlighted in Fig. 5 and confirms the fast decay of kinetic energy in beam 1 and increase in beam 2. The reverse energy flow, however, is eliminated by switching off the parametric excitation, which generates a single pulse of parametric excitation. The general idea was outlined already in [29].

6 Multiple parametric excitations in 3DOF

The concept of reducing the settling time by a duplication of the structure is extended to more beams. It is straightforward to do this numerically. However, for a practical implementation, we need to know the time period(s) of the pulsed parametric excitations upfront. For this, we apply the averaging method to a system consisting of three beams, one sensing beam and two structural duplicates possessing similar but not exactly the same natural frequencies. With three beams, we have more than one possibility of transferring energy between the first modes of each beam, so we introduce a quasi-periodic parametric excitation of the form

$$\ddot{\mathbf{x}} + \boldsymbol{D}\dot{\mathbf{x}} + \left(\boldsymbol{\Omega}^2 + \mathbf{B}\left[\cos\left(\Omega_p^{21} t\right) + \cos\left(\Omega_p^{31} t\right)\right]\right)\mathbf{x} = 0 \tag{23}$$

where $\mathbf{x} = \left[x_1\ x_2\ x_3\right]^T$, $\Omega^2 = \mathrm{diag}\left\{\Omega_1^2, \Omega_2^2, \Omega_3^2\right\}$ and $\boldsymbol{D} = \begin{bmatrix} d_{11} & d_{12} & d_{13} \\ d_{21} & d_{22} & d_{23} \\ d_{31} & d_{32} & d_{33} \end{bmatrix}$ and $\boldsymbol{B} = \begin{bmatrix} b_{11} & b_{12} & b_{13} \\ b_{21} & b_{22} & b_{23} \\ b_{31} & b_{32} & b_{33} \end{bmatrix}$ being fully occupied coefficient matrices for damping and time-periodic coupling. The parametric exci-

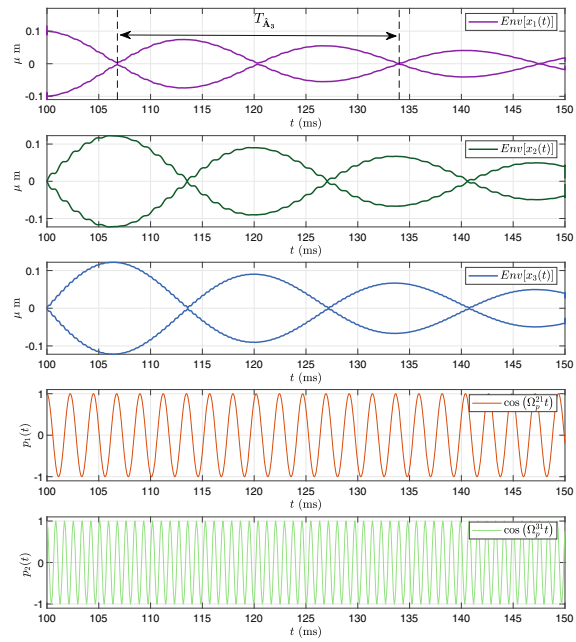

Fig. 6 Envelope of the time responses of the 3DOF-MEMS in Eq. (23) at continuous, quasi-periodic parametric excitation Ω_p^{21} and Ω_p^{31}. The analytical prediction in Eq. (29) matches the observed period $T_{\hat{\mathbf{A}}_3}$

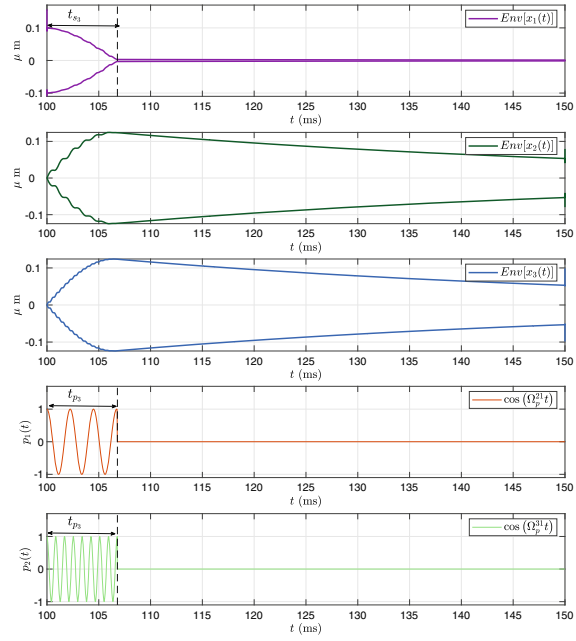

Fig. 7 Envelope of the time responses of the 3DOF-MEMS in Eq. (23) at quasi-periodic parametric excitation Ω_p^{21} and Ω_p^{31} pulsed during t_{p_3} predicted in Eq. (29). The settling time reduces to t_{s_3}

tation consists of two periodic signals that are tuned each at a parametric anti-resonance frequency: $\Omega_p^{21} = |\Omega_2 - \Omega_1|$ and $\Omega_p^{31} = |\Omega_3 - \Omega_1|$. The system in Eq. (23) describes a dynamic system with a multiple parametric excitation, a quasi-periodic parametric excitation.

Given the identical structure of the MEMS considered, each flexible beam has similar quality factors $Q_i = \Omega_i/d_{ii}$. To simplify the subsequent analysis, it is assumed that each beam possesses the same direct damping coefficient, i.e. $d_{11} = d_{22} = d_{33} = d$. Applying the averaging method described in the previous section on the system in Eq. (23) with the time rescaling

$$\tau = \Omega_p^{21} t, \tag{24}$$

the following slow flow is obtained

$$\hat{\mathbf{z}}_{\mathbf{3}}{}'(\tau) = \hat{\mathbf{A}}_{\mathbf{3}}\hat{\mathbf{z}}_{\mathbf{3}}(\tau) \tag{25}$$

with the coefficients matrix

$$\hat{\mathbf{A}}_{\mathbf{3}} = \frac{1}{\Omega_p^{21}} \begin{bmatrix} -\frac{d}{2} & 0 & 0 & \frac{b_{12}}{4\Omega_1} & 0 & \frac{b_{13}}{4\Omega_1} \\ 0 & -\frac{d}{2} & -\frac{b_{12}}{4\Omega_1} & 0 & -\frac{b_{13}}{4\Omega_1} & 0 \\ 0 & \frac{b_{21}}{4\Omega_2} & -\frac{d}{2} & 0 & 0 & 0 \\ -\frac{b_{21}}{4\Omega_2} & 0 & 0 & -\frac{d}{2} & 0 & 0 \\ 0 & \frac{b_{31}}{4\Omega_3} & 0 & 0 & -\frac{d}{2} & 0 \\ -\frac{b_{31}}{4\Omega_3} & 0 & 0 & 0 & 0 & -\frac{d}{2} \end{bmatrix}. \tag{26}$$

The coefficient matrix for the 2DOF-system in Eq. (18) can be identified as a submatrix. Again, only the diagonal damping coefficients and the coupling terms are needed for describing the slow in this first order approximation. For the chosen parametric excitation frequencies Ω_p^{21} and Ω_p^{31} this results in b_{12}, b_{21} and b_{13}, b_{31}. Since $b_{ij} > 0$ and $d > 0$ hold for this specific MEMS configuration, the coefficient matrix $\hat{\mathbf{A}}_{\mathbf{3}}$ has two repeated purely real-valued eigenvalues

$$\lambda_1^{\hat{\mathbf{A}}_{\mathbf{3}}} = \lambda_2^{\hat{\mathbf{A}}_{\mathbf{3}}} = -\frac{d}{2\Omega_p^{21}} \tag{27}$$

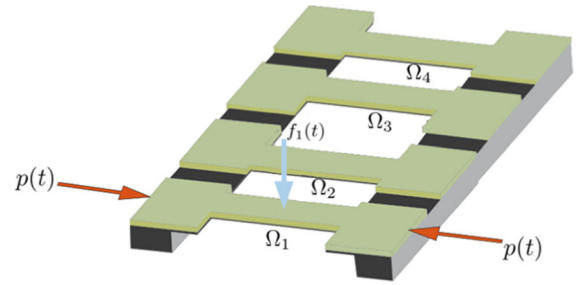

Fig. 8 MEMS schematic diagram with 4DOF

and two repeated pairs of complex conjugates

$$\lambda_{34}^{\hat{\mathbf{A}}_{\mathbf{3}}} = \lambda_{56}^{\hat{\mathbf{A}}_{\mathbf{3}}} = \frac{1}{2\Omega_p^{21}} \left(-d \pm j \sqrt{\frac{b_{13}b_{31}}{4\Omega_1\Omega_3} + \frac{b_{12}b_{21}}{4\Omega_1\Omega_2}} \right)$$

For $b_{ij} > 0$ and $d > 0$, the frequency of the slow flow reads

$$\hat{\omega}_{\hat{\mathbf{A}}_3} = \frac{1}{2\Omega_p^{21}} \sqrt{\frac{b_{12}b_{21}}{4\Omega_1\Omega_2} + \frac{b_{13}b_{31}}{4\Omega_1\Omega_3}} \tag{28}$$

The prediction of the period of the slow flow of the system response in Eq. (23) is obtained by rescaling the time to the original physical time according to Eq. (24)

$$T_{\hat{\mathbf{A}}_3} = 4\pi \sqrt{\frac{4\Omega_1\Omega_2\Omega_3}{\Omega_3 b_{12}b_{21} + \Omega_2 b_{13}b_{31}}} = 4t_{p_3} \tag{29}$$

Herein, t_{p_3} is the pulse time for achieving an energy transfer from beam 1 to beam 2 and beam 3 simultanously. The envelopes of the time responses of the 3DOF-MEMS in Eq. (23) at continuous, quasi-periodic parametric excitation Ω_p^{21} and Ω_p^{31} are shown in Fig. 6. The period $T_{\hat{\mathbf{A}}_3}$ coincides with the analytical prediction in Eq. (29). Envelope of the very same system but activating the quasi-periodic parametric excitation only during the pulsation time t_{p_3} defined in Eq. (29) reduces the settling time to $t_{p_3} = 6.8$ ms and is shown in Fig. 7.

7 Multiple parametric excitations in 4DOF

Attempting to generalize the reduction of settling time presented for 2DOF-MEMS and 3DOF-MEMS, the 3DOF-MEMS in the previous section is extended

by an additional beam with nominally identical parameters, see Fig. 8. By adding another beam to the structure, the system now consists of one sensing beam and three duplicates. This configuration is expected to allow for further reduction of the settling time because one additional parametric anti-resonance frequency is introduced.

For a MEMS with four beams, the equations of motion read

$$\ddot{\mathbf{x}} + \boldsymbol{D}\dot{\mathbf{x}} + \left(\boldsymbol{\Omega}^2 + \mathbf{B}p(t)\right)\mathbf{x} = 0 \tag{30}$$

Herein, $\mathbf{x} = \left[x_1\ x_2\ x_3\ x_4\right]^T$, Ω^2 is the diagonal matrix of the natural frequencies of the underlying system with constant coefficients and the damping and coupling coefficient matrices are fully occupied and of size 4×4, and the parametric excitation $p(t)$ is the sum harmonic parametric excitations at each parametric anti-resonance frequency that enables an energy transfer with beam 1. For a 4DOF-MEMS, the quasi-periodic parametric excitation consists of three harmonics

$$p(t) = \cos\left(\Omega_p^{21}t\right) + \cos\left(\Omega_p^{31}t\right) + \cos\left(\Omega_p^{41}t\right) \tag{31}$$

experiencing the parametric anti-resonance frequencies $\Omega_p^{21} = |\Omega_2 - \Omega_1|$, $\Omega_p^{31} = |\Omega_3 - \Omega_1|$ and $\Omega_p^{41} = |\Omega_4 - \Omega_1|$. Averaging the equations of motion in Eq. (30) for the system in Fig. 8 yields

$$\hat{\mathbf{z}}_{\mathbf{4}}{}'(\tau) = \hat{\mathbf{A}}_{\mathbf{4}}\hat{\mathbf{z}}_{\mathbf{4}}(\tau) \tag{32}$$

with the coefficients matrix

$$\hat{\mathbf{A}}_4 = \frac{1}{\Omega_p^{21}}\begin{bmatrix} \frac{-d}{2} & 0 & 0 & \frac{b_{12}}{4\Omega_1} & 0 & \frac{b_{13}}{4\Omega_1} & 0 & \frac{b_{14}}{4\Omega_1} \\ 0 & \frac{-d}{2} & \frac{-b_{12}}{4\Omega_1} & 0 & \frac{-b_{13}}{4\Omega_1} & 0 & \frac{-b_{14}}{4\Omega_1} & 0 \\ 0 & \frac{b_{21}}{4\Omega_2} & \frac{-d}{2} & 0 & 0 & 0 & 0 & 0 \\ \frac{-b_{21}}{4\Omega_2} & 0 & 0 & \frac{-d}{2} & 0 & 0 & 0 & 0 \\ 0 & \frac{b_{31}}{4\Omega_3} & 0 & 0 & \frac{-d}{2} & 0 & 0 & 0 \\ \frac{-b_{31}}{4\Omega_3} & 0 & 0 & 0 & 0 & \frac{-d}{2} & 0 & 0 \\ 0 & \frac{-b_{41}}{4\Omega_4} & 0 & 0 & 0 & 0 & \frac{-d}{2} & 0 \\ \frac{-b_{41}}{4\Omega_4} & 0 & 0 & 0 & 0 & 0 & 0 & \frac{-d}{2} \end{bmatrix} \tag{33}$$

The time was rescaled by applying $\tau = \Omega_p^{21}t$ similarly to Eq. (4) and the direct damping coefficients were assumed to be identical $d_{11} = d_{22} = d_{33} = d_{44} = d$. The coefficient matrices for the 2DOF-system in Eq. (17) and for the 3DOF-system in Eq. (26) can be identified as submatrices. Similarly to the last sections, the only coefficients that describe the dynamics of the slow flow in a first order approximation of the quasi-periodic parametric excitation are the direct damping coefficients d and the coupling coefficients (b_{12}, b_{21}), (b_{13}, b_{31}), (b_{14}, b_{41}). These coupling coefficients correspond to the parametric anti-resonance frequencies Ω_p^{21}, Ω_p^{31} and Ω_p^{41}, respectively, to which the harmonic components in Eq. (31) are perfectly tuned to.

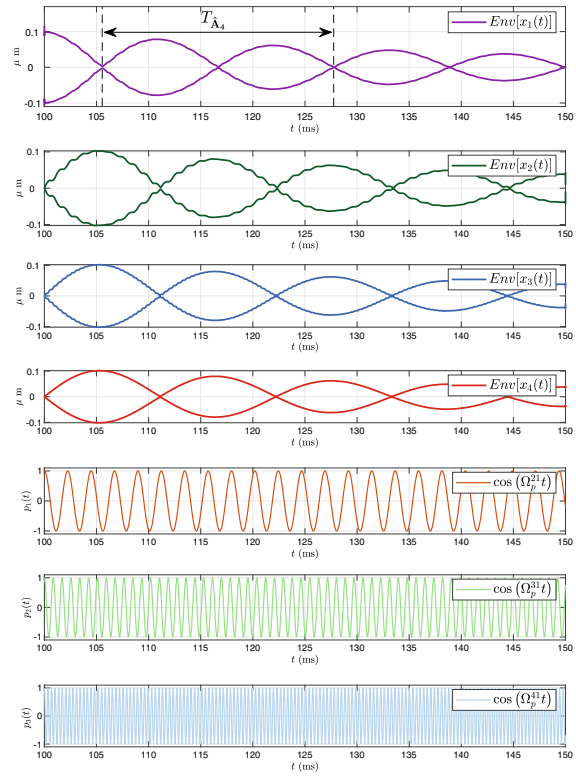

Fig. 9 Envelope of the time responses of the 4DOF-MEMS in Eq. (30) at Ω_p^{21}, Ω_p^{31} and Ω_p^{41}. The analytical prediction in Eq. (35) matches the observed period $T_{\hat{\mathbf{A}}_4}$

The coefficient matrix $\hat{\mathbf{A}}_4$ has four repeated purely real-valued eigenvalues $\lambda_{1234}^{\hat{\mathbf{A}}_4}$, that are identical to Eq. (27), and two repeated pairs of complex conjugates

$$\lambda_{5678}^{\hat{\mathbf{A}}_4} = -\frac{d}{2\Omega_p^{21}} \pm j\hat{\omega}_{\hat{\mathbf{A}}_4}$$

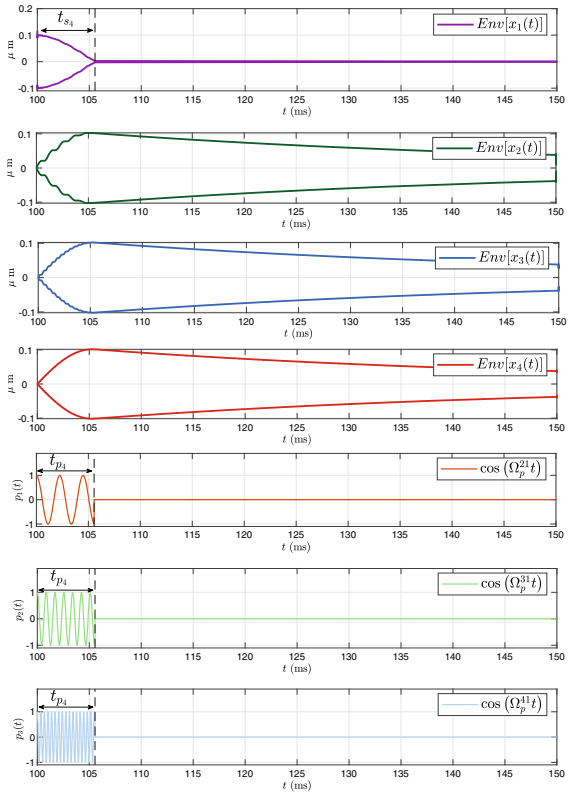

Fig. 10 Envelope of the time responses of the 4DOF-MEMS under the pulses of excitation $\Omega_p^{21} = |\Omega_2 - \Omega_1|$, $\Omega_p^{31} = |\Omega_3 - \Omega_1|$ and $\Omega_p^{41} = |\Omega_4 - \Omega_1|$ for t_{p_4} in Eq. (35). The settling time reduces to t_{s_4}

The frequency of the slow flow reads similarly to Eq. (28)

$$\hat{\omega}_{\hat{\mathbf{A}}_4} = \frac{1}{2\Omega_p^{21}}\sqrt{\frac{b_{12}b_{21}}{4\Omega_1\Omega_2} + \frac{b_{13}b_{31}}{4\Omega_1\Omega_3} + \frac{b_{14}b_{41}}{4\Omega_2\Omega_3}} \tag{34}$$

The period of the envelope of slow dynamics becomes in physical time

$$T_{\hat{\mathbf{A}}_4} = 4\pi\sqrt{\frac{4\Omega_1\Omega_2\Omega_3\Omega_4}{\Omega_3\Omega_4 b_{12}b_{21} + \Omega_2\Omega_4 b_{13}b_{31} + \Omega_2\Omega_3 b_{14}b_{41}}} \tag{35}$$

The pulse time results in $t_{p_4} = T_{\hat{\mathbf{A}}_4}/4$ during which an energy transfer from beam 1 to beam 2, beam 3 and beam 4 is achieved simultanously. The envelopes of the time responses of a 4DOF-MEMS at continuous, quasi-periodic parametric excitation Ω_p^{21}, Ω_p^{31} and Ω_p^{41} are shown in Fig. 9. The system parameters are listed in the first four lines in Table 2. The period $T_{\hat{\mathbf{A}}_4}$ coincides with the analytical prediction in Eq. (35). The Envelope of the very same system but activating the quasi-periodic parametric excitation only during the pulsation time t_{p_4} defined in Eq. (35) reduces the settling time to 5.6 ms and is shown in Fig. 10.

8 Multiple parametric excitations in NDOF

In general, for an arbitrary number of beams m, the equations of motion are equivalent to Eq. (30). Herein, $\mathbf{x} = \begin{bmatrix} x_1 & x_2 & \dots & x_m \end{bmatrix}^T$, Ω^2 is the diagonal matrix of the natural frequencies of the underlying system with constant coefficients and the damping and coupling coefficient matrices are fully occupied and of size $m \times m$ and the parametric excitation is the sum harmonic parametric excitations at each parametric anti-resonance frequency $\Omega_p^{i1} = |\Omega_i - \Omega_1|$ that enables an energy transfer with beam 1,

$$p(t) = \sum_{i=2}^{m} \cos(\Omega_p^{i1} t) \tag{36}$$

We attempt an approximation of the period for energy transfer at this highly tuned quasi-periodic parametric excitation based on the structure observed in Eqs. (22), (29) and (35). For a MEMS design similar to the one shown in Fig. 8 consisting of m similar beams, the period for energy transfer appears to be

$$T_{\hat{\mathbf{A}}_\mathbf{m}} = \frac{4\pi}{\sqrt{\sum_{i=2}^{m} \frac{b_{1i}b_{i1}}{4\Omega_1\Omega_i}}} = 4t_{pN} \tag{37}$$

The analytical prediction in Eq. (37) is tested for NDOF-MEMS with one to nine beam duplicates, e.g. MEMS possessing two to ten DOF. The envelope response of the sensing beam 1 is shown in Fig. 11. The system parameters are chosen according to the values listed in Table 2. The decrease of the settling time, the time for energy transfer from beam 1 to all other beams by a pulsed quasi-periodic parametric excitation is clearly highlighted. Finally, we compare the pulse time t_{pN}, or equivalently settling time of the NDOF-MEMS, to the analytical prediction in

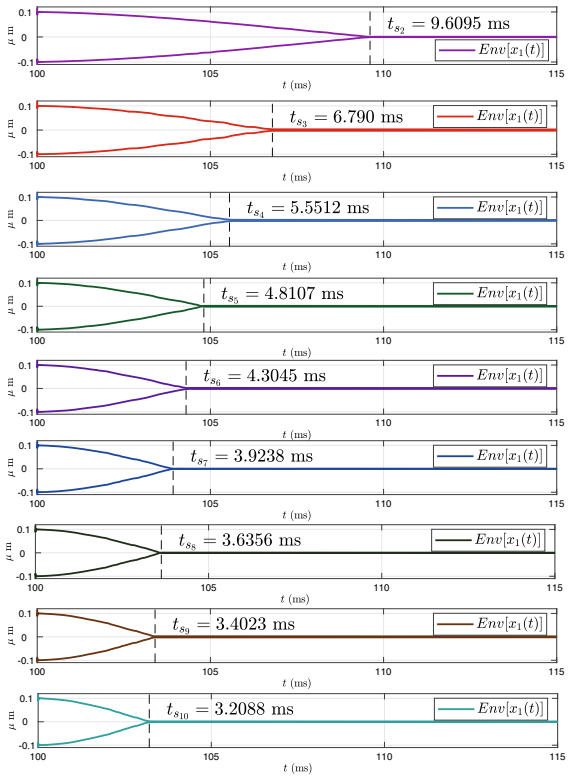

Fig. 11 Envelope of the time responses of the NDOF- MEMS starting with 2DOF in Fig. 5, 3DOF in Fig. 7, 4DOF in Fig. 10 up to 10DOF. Parameter values are according to Table 2

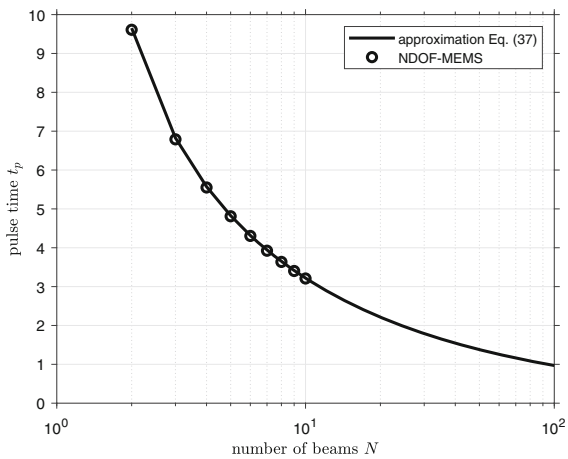

Fig. 12 Pulse or settling time in dependency of the number of beams: derivation from numerical time integration of the equations motion according to Fig. 11 in comparison to the analytical approximation in Eq. (37)

Eq. (37) in Fig. 12. The analytical prediction fits perfectly to the settling time derived from the direct numerical integration of the equations of motion for the individual MEMS-configurations in Fig. 11. This comparison confirms that in the case of identical beams, the settling time is proportional to $1/\sqrt{N}$. The diagram allows for an extrapolation of the number of beams N of the NDOF-MEMS and provides an answer on how many similar beams are needed for achieving a certain settling time.

9 Conclusions

The parametric anti-resonance concept is generalized to a multi-frequency, pulsed parametric excitation in a multi-degree-of-freedom system in order to achieve a reduction in the settling time in a specific system. This open-loop control applies one or more intentional, confined (pulsed), harmonic parametric excitations. If properly tuned, a significant reduction of the transient time is achieved. MEMS show promising applicability of this concept due to the ability to easily introduce periodic and quasi-periodic signals tuned to a specific frequency. This concept triggers multiple simultaneous energy transfers from the sensing mode of beam 1 to several beams. The selectivity of which beams are incorporated in an energy transfer is purely controlled by the individually chosen excitation frequency and coupling terms. The concept was shown originally in [29] for two beams with a single-frequent parametric excitation at $\Omega_p^{21} = |\Omega_2 - \Omega_1|$. Here we greatly enhance the applicability as well as complexity by introducing N beams and multiple pulses of parametric excitation at $\Omega_p^{i1} = |\Omega_i - \Omega_1|$ with $i = 2, 3, \ldots N$. The averaging method in the general case is applied to achieve an analytical prediction at very specific excitation frequencies. The approximate slow flow dynamics can accurately predict the pulsation time needed for such a quasi-periodic parametric excitation. This allows for properly designing the necessary pulse for rapid energy transfer between system modes or individual beams, which eventually leads to mitigating the kinetic energy, and therefore settling time, of the first mode. The newly proposed method is applied to the arrays of MEMS consisting of flexible beams with high quality factors. Such beams are prone to long steady-state transition times that may be too long for certain fast, repetitive operations. The influence of the number

Table 2 Paramaters for NDOF-system

Ω_i in Mrad/s	$Q\ [\times 10^4]$	b_{ij} in 1/s^2
$\Omega_1 = 1.8316$	$Q_1 = 4.6964$	$b_{12} = b_{21} = 1.2 \times 10^9$
$\Omega_2 = 1.8344$	$Q_2 = 4.7036$	$b_{13} = b_{31} = 1.3 \times 10^9$
$\Omega_3 = 1.8390$	$Q_3 = 4.7154$	$b_{14} = b_{41} = 1.2 \times 10^9$
$\Omega_4 = 1.8499$	$Q_4 = 4.7433$	$b_{15} = b_{51} = 1.2 \times 10^9$
$\Omega_5 = 1.8512$	$Q_5 = 4.7467$	$b_{16} = b_{61} = 1.2 \times 10^9$
$\Omega_6 = 1.8210$	$Q_6 = 4.6694$	$b_{17} = b_{71} = 1.3 \times 10^9$
$\Omega_7 = 1.8433$	$Q_7 = 4.7264$	$b_{18} = b_{81} = 1.2 \times 10^9$
$\Omega_8 = 1.8601$	$Q_8 = 4.7695$	$b_{19} = b_{91} = 1.2 \times 10^9$
$\Omega_9 = 1.8555$	$Q_9 = 4.7577$	$b_{12} = b_{11} = 1.2 \times 10^9$
$\Omega_{10} = 1.8255$	$Q_{10} = 4.6808$	$b_{1_{10}} = b_{10_1} = 1.2 \times 10^9$

The diagonal terms are $b_{kk} = 1.2 \times 10^9$ for $k = 1, \ldots, 10$ and the remaining coupling terms $b_{i,j} = b_{j,i} = 1.3 \times 10^9$ for $i = 2, \ldots, 10$, $j = 2, \ldots, 10$ and $i \neq j$

of beams in the MEMS is evaluated in more detail and shows that the original reduction of the settling time by 90.39% for a 2DOF-MEMS is reduced to 93.13% for a 3DOF-MEMS, to 94.44% for a 4DOF-MEMS and to 96.79% for a 10DOF-MEMS. This study confirms that a designed pulse of multi-frequency parametric excitation reduces the settling time significantly.

Acknowledgements The author MRB thanks the IPN-SIP-202315 and the Austrian Academy of Sciences for their support for the development of this project.

Funding This work was supported by the Joint Excellence in Science and Humanities (JESH) programme of the Austrian Academy of Sciences through the grant given to the first author.

Data availability The authors declare that all data supporting the simulations and examples of this study are available within the article.

Declarations

Conflict of interest The authors declare that they have no conflict of interest.

Appendix

The solution $x_1(t)$ of beam 1 of the original systems for configurations with 2DOF, 3DOF and 4DOF defined in Eqs. (16), (23) and (30) is compared directly with the solution $|\hat{u_1}|$ of the approximated slow flows in Eqs. (17), (25) and (32). This is possible due to the definition in Eq. (6). The solutions are transformed according to Eq. (4) into the physical time t. The system parameters are taken from the list given in Table 2. The initial condition is chosen as $x_1(0) = 0$ in all cases. Figure 13 highlights the quality of the approximation between the physical time evolution and the envelope represented by the slow flow.

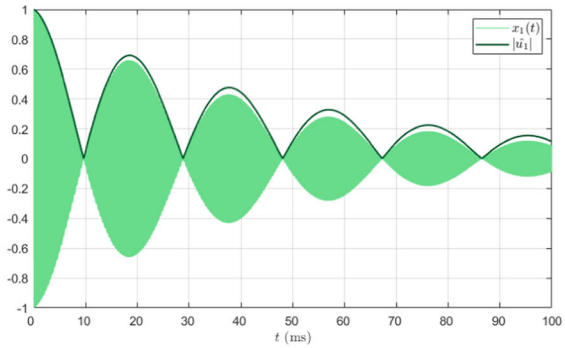

(a) Configuration with 2DOF in Eqs. (16) and (17).

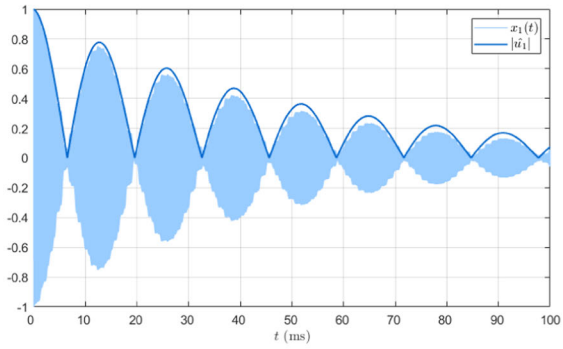

(b) Configuration with 3DOF in Eqs. (23) and (25).

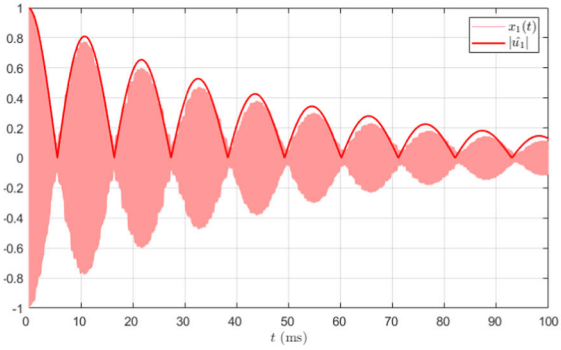

(c) Configuration with 4DOF in Eqs. (30) and (32).

Fig. 13 Comparison between the full solution $x_1(t)$ of the original system and the envelope $|\hat{u}_1|$ of the approximate system

References

1. Almog, R., Zaitsev, S., Shtempluck, O., Buks, E.: High intermodulation gain in a micromechanical Duffing resonator. Appl. Phys. Lett. (2006). https://doi.org/10.1063/1.2207490
2. Andreaus, U., Dell'Isola, F., Porfiri, M.: Piezoelectric passive distributed controllers for beam flexural vibrations. J. Vib. Control **10**(5), 625–659 (2004). https://doi.org/10.1177/1077546304038224
3. Asadi, K., Yu, J., Cho, H.: Nonlinear couplings and energy transfers in micro-and nano-mechanical resonators: intermodal coupling, internal resonance and synchronization. Philos. Trans. R. Soc. A Math. Phys. Eng. Sci. **376**(2127), 20170141 (2018)
4. Bayer, F., Leine, R.I.: Sorting-free hill-based stability analysis of periodic solutions through koopman analysi. Nonlinear Dyn. **111**(1), 1–9 (2023). https://doi.org/10.1007/s11071-023-08247-7
5. Cartmell, M.: Introduction to Linear, Parametric and Non-Linear Vibrations, 1st edn. Chapman and Hall, Boca Raton (1990)
6. Chen, C., Zanette, D.H., Czaplewski, D.A., Shaw, S., López, D.: Direct observation of coherent energy transfer in nonlinear micromechanical oscillators. Nat. Commun. **8**(1), 15523 (2017)
7. Choudhary, V., Iniewski, K.: Mems: fundamental technology and applications. CRC Press, Boca Raton (2017)
8. Collado, J.: Hill Equation. From 1 to 2 Degrees of Freedom, pp. 43–71. Springer International Publishing, Cham (2018). https://doi.org/10.1007/978-3-319-62464-8_3
9. Dick, N., Krylov, S.: Parametric resonance and pattern selection in an array of microcantilevers interacting through fringing electrostatic fields. Nonlinear Dyn. (2021). https://doi.org/10.1007/s11071-021-06755-y
10. Dohnal, F.: Damping by parametric stiffness excitation: resonance and anti-resonance. J. Vib. Control **14**(5), 669–688 (2008). https://doi.org/10.1177/1077546307082983
11. Dohnal, F.: General parametric stiffness excitation-anti-resonance frequency and symmetry. Acta Mech. **196**(1–2), 15–31 (2008). https://doi.org/10.1007/s00707-007-0497-x
12. Dohnal, F.: Optimal dynamic stabilisation of a linear system by periodic stiffness excitation. J. Sound Vib. **320**(4), 777–792 (2009). https://doi.org/10.1016/j.jsv.2008.09.020
13. Dohnal, F.: Experimental studies on damping by parametric excitation using electromagnets. Proc. Inst. Mech. Eng. C J. Mech. Eng. Sci. **226**(8), 2015–2027 (2012)
14. Dohnal, F., Tondl, A.: Using time-periodicity for inducing energy transfer between vibration modes. In: International Design Engineering Technical Conferences and Computers and Information in Engineering Conference, vol. 55973. American Society of Mechanical Engineers (2013)
15. Dohnal, F., Verhulst, F.: Averaging in vibration suppression by parametric stiffness excitation. Nonlinear Dyn. **54**(3), 231–248 (2008). https://doi.org/10.1007/s11071-007-9325-z
16. Fossen, T., Nijmeijer, H.: Parametric resonance in dynamical systems. Sci. Bus. Media (2011). https://doi.org/10.1007/978-1-4614-1043-0
17. Hajjaj, A., Jaber, N., Ilyas, S., Alfosail, F., Younis, M.: Linear and nonlinear dynamics of micro and nano-resonators:

review of recent advances. Int. J. Non-Linear Mech. **119**, 103328 (2020). https://doi.org/10.1016/j.ijnonlinmec.2019.103328
18. Kovaleva, M., Manevitch, L., Romeo, F.: Stationary and non-stationary oscillatory dynamics of the parametric pendulum. Commun. Nonlinear Sci. Numer. Simul. **76**, 1–11 (2019). https://doi.org/10.1016/j.cnsns.2019.02.016
19. Lacarbonara, W.: Nonlinear structural mechanics: theory, dynamical phenomena and modeling. Sci. Bus. Media (2013). https://doi.org/10.1007/978-1-4419-1276-3
20. Mahboob, I., Nishiguchi, K., Okamoto, H., Yamaguchi, H.: Phonon-cavity electromechanics. Nat. Phys. **8**(5), 387 (2012). https://doi.org/10.1038/nphys2277
21. Mahboob, I., Yamaguchi, H.: Bit storage and bit flip operations in an electromechanical oscillator. Nat. Nanotechnol. **3**(5), 275 (2008). https://doi.org/10.1038/nnano.2008.84
22. Maurini, C., dell'Isola, F., Del Vescovo, D.: Comparison of piezoelectronic networks acting as distributed vibration absorbers. Mech. Syst. Signal Process. **18**(5), 1243–1271 (2004). https://doi.org/10.1016/S0888-3270(03)00082-7
23. Moran, K., Burgner, C., Shaw, S., Turner, K.: A review of parametric resonance in microelectromechanical systems. Nonlinear Theory Appl. IEICE **4**(3), 198–224 (2013). https://doi.org/10.1587/nolta.4.198
24. Nayfeh, A.H., Mook, D.T.: Nonlinear oscillations. Wiley, London (1995)
25. Okamoto, H., Gourgout, A., Chang, C.Y., Onomitsu, K., Mahboob, I., Chang, E.Y., Yamaguchi, H.: Coherent phonon manipulation in coupled mechanical resonators. Nat. Phys. **9**(8), 480 (2013). https://doi.org/10.1038/nphys2665
26. Okamoto, H., Mahboob, I., Onomitsu, K., Yamaguchi, H.: Rapid switching in high-Q mechanical resonators. Appl. Phys. Lett. (2014). https://doi.org/10.1063/1.4894417
27. Ramírez-Barrios, M., Collado, J., Dohnal, F.: Coupled mathieu equations: γ-hamiltonian and μ-symplectic. Dyn. Syst. Theory. IntechOpen (2019). https://doi.org/10.5772/intechopen.88635
28. Ramírez-Barrios, M., Collado, J., Dohnal, F.: Stability of coupled and damped mathieu equations utilizing symplectic properties. In: W. Lacarbonara, B. Balachandran, J. Ma, J.A. Tenreiro Machado, G. Stepan (eds.) Nonlinear Dynamics of Structures, Systems and Devices, pp. 137–145. Springer International Publishing, Cham (2020). https://doi.org/10.1007/978-3-030-34713-0_14
29. Ramírez-Barrios, M., Dohnal, F., Collado, J.: Enhanced vibration decay in high-q resonators by confined of parametric excitation. Arch. Appl. Mech. **90**(8), 1673–1684 (2020). https://doi.org/10.1007/s00419-020-01689-0
30. Ramírez-Barrios, M., Dohnal, F., Collado, J.: Transient vibrations suppression in parametrically excited resonators. In: Hernandez, E.E., Keshtkar, S., Valdez, S.I. (eds.) Industrial and Robotic Systems, pp. 193–205. Springer International Publishing, Cham (2020). https://doi.org/10.1007/978-3-030-45402-9_19
31. Rand, R., Morrison, T.: 2:1:1 resonance in the quasi-periodic mathieu equation. Nonlinear Dyn. **40**, 195–203 (2005). https://doi.org/10.1007/s11071-005-6005-8
32. Rhoads, J.F., Shaw, S.W., Turner, K.L., Moehlis, J., DeMartini, B.E., Zhang, W.: Generalized parametric resonance in electrostatically actuated microelectromechanical oscillators. J. Sound Vib. **296**(4), 797–829 (2006). https://doi.org/10.1016/j.jsv.2006.03.009
33. Rossing, T.D., Fletcher, N.H., Tubis, A.: Principles of Vibration and Sound, 2nd edition. J. Acoust. Soc. Am. **116**(5), 2708–2708 (2004). https://doi.org/10.1121/1.1810535
34. Shoshani, O., Shaw, S.W.: Resonant modal interactions in micro/nano-mechanical structures. Nonlinear Dyn. **104**, 1801–1828 (2021)
35. Thomsen, J.J.: Vibrations and stability: advanced theory, analysis, and tools. Springer, Cham (2021). https://doi.org/10.1007/978-3-030-68045-9
36. Tondl, A.: Quenching of self-excited vibrations equilibrium aspects. J. Sound Vib. **42**(2), 251–260 (1975). https://doi.org/10.1016/0022-460X(75)90220-5
37. Tongue, B.H.: Principles of vibration. Oxford University Press, USA (2002)
38. Vakakis, A.F., Gendelman, O.: Energy pumping in nonlinear mechanical oscillators: Part II-resonance capture. J. Appl. Mech. **68**(1), 42–48 (2000). https://doi.org/10.1115/1.1345525
39. Verhulst, F.: Nonlinear differential equations and dynamical systems. Springer, Berlin (2006)
40. Verhulst, F.: Multiple timing and spatial scaling for bifurcations. Nonlinear Dyn. **111**(12), 10693–10707 (2023). https://doi.org/10.1007/s11071-023-08378-x
41. Voiculescu, I., Nordin, A.N.: Acoustic wave based mems devices for biosensing applications. Biosens. Bioelectron. **33**(1), 1–9 (2012). https://doi.org/10.1016/j.bios.2011.12.041
42. Wooden, S.M., Sinha, S.: Analysis of periodic-quasiperiodic nonlinear systems via lyapunov-floquet transformation and normal forms. Nonlinear Dyn. **47**, 263–273 (2007). https://doi.org/10.1007/s11071-006-9072-6
43. Yakubovich, V., Starzhinskii, V.: Linear Differential Equations With Periodic Coefficients, vol. 1,2. Wiley, London (1975)
44. Younis, M.I.: MEMS linear and nonlinear statics and dynamics, vol. 20. Springer, Berlin (2011)
45. Zounes, R.S., Rand, R.H.: Global behavior of a nonlinear quasiperiodic mathieu equation. Nonlinear Dyn. **27**, 87–105 (2002). https://doi.org/10.1023/A:1017931712099